



Electrodeposited ZnO Nanowires as Photoelectrode in Solid-State Organic Dye-Sensitized Solar Cells

Journal:	<i>Physical Chemistry Chemical Physics</i>
Manuscript ID:	CP-ART-10-2013-054210.R2
Article Type:	Paper
Date Submitted by the Author:	28-Feb-2014
Complete List of Authors:	Muguerra, Hervé; CEA, INAC Berthoux, Gaelle; CEA, INAC Yahya, Wan Zaireen Nisa; CEA, INAC Kervella, Yann; CEA, INAC Ivanova, Valentina; CEA-Leti, Bouclé, Johann; Université de Limoges, XLIM DEMADRILLE, Renaud; CEA, INAC

Electrodeposited ZnO Nanowires as Photoelectrode in Solid-State Organic Dye-Sensitized Solar Cells

Cite this: DOI: 10.1039/x0xx00000x

Hervé Muguerra,^a Gaëlle Berthoux,^a Wan Zaireen Nisa Yahya,^a Yann Kervella,^a Valentina Ivanova,^b Johann Bouclé*^c and Renaud Demadrille*^a

Received 07th October 2013,
Accepted 00th xx 201x

DOI: 10.1039/x0xx00000x

www.rsc.org/

A new approach for developing solid-state dye-sensitized solar cells (DSSCs) on Glass/ITO and plastic substrates (PEN/ITO) is presented in this manuscript. A two steps electrodeposition technique has been employed to realize the ZnO photoelectrodes. First a ZnO thin film is deposited on ITO substrate and subsequently on this buffer layer ZnO nanowires of 650 nm long are grown. The different nanostructured electrodes are crystallized and show a transparency close to 80% in the visible spectral range. The electrodes are then sensitized with a new purely organic dye, whose synthesis is presented here, which reveals a wide absorption spectrum and high molar extinction coefficient. Finally, the sensitized electrodes were employed for the fabrication of liquid and solid-state DSSCs, using respectively a liquid iodine/iodide electrolyte and the Spiro-OMeTAD hole transporter. These devices represent the first solid-state DSSCs fabricated with electrodeposited zinc oxide nanowires. Their power conversion efficiency are still limited, respectively 0.18% and 0.03% under standard AM 1.5G sunlight (100 mW cm⁻²), nevertheless these results prove the interest of this low-temperature deposition method for the realization of nanostructured electrodes on rigid and flexible substrates, and open new perspectives for the development of solid state DSSCs on plastic substrates.

1. Introduction

Dye-Sensitized Solar Cells (DSSCs) appeared in the last decades as a promising technology for energy conversion due to their convenient and low cost fabrication process, and their relatively high efficiency.¹⁻³ Compared to other solar cells technologies, DSSCs present many advantages: they can be fabricated by simple screen printing methods and do not have to undergo costly purification steps or doping treatments, besides they usually employ low toxicity materials.⁴ DSSCs are photo-electrochemical devices which combine a wide band gap semiconducting nanostructured oxide film, such as Titanium dioxide (TiO₂) or Zinc oxide (ZnO) as photoelectrode and organic complexes or metal-free dyes as sensitizers.^{1,5} The photoelectric conversion efficiency of DSSCs based on TiO₂ photoanodes has reached values as high as 12.3% under simulated air mass 1.5 global sunlight.⁶ Despite of the fact that the champion cells are fabricated using nanostructures made of TiO₂, other binary metal oxide have been successfully used as photo-electrodes in DSSCs such as SnO₂,⁷ Nb₂O₅,⁸ and In₂O₃⁹ and among them ZnO appears as alternative material for the fabrication of high efficiency DSSCs. Indeed, using ZnO nanoparticles, power conversion efficiencies up to 7.5% have been obtained.¹⁰

ZnO is a wide band gap semiconducting material (3.37 eV) with a conduction band edge very close to that of TiO₂ (*ca* -4.4 eV). This material possesses a good stability and it exhibits electron mobility in the bulk 2 - 3 orders of magnitude higher than that of TiO₂.¹¹ However devices based on ZnO usually show significantly smaller open-circuit voltages mainly because charge recombination processes are slightly accelerated in this material compared to TiO₂.¹² Nevertheless, ZnO is still very attractive due to the

possibility to be prepared in a large diversity of nanostructures such as nanoparticles,^{13,4} nanosheets,¹⁵ nanowires,^{16,17} or tetrapods.¹⁸ In addition, different synthetic routes can be employed to fabricate ZnO electrodes and one can cite hydrothermal synthesis,¹⁹ electrochemical deposition,²⁰ spray pyrolysis,²¹ polyol hydrolysis²² and chemical vapor deposition.²³ Unfortunately most of these techniques require post-deposition annealing steps and consequently they are not compatible with the fabrication of DSSCs on flexible substrates. Due to this reason the literature concerning the fabrication of flexible dye-sensitized solar cells with ZnO is really scarce.²⁴ In this paper, we report on the preparation of ZnO nanowire-based photoelectrodes by electrochemical deposition on rigid and flexible substrates. The potentiality of these ZnO electrodes for the fabrication of DSSCs is also investigated. The electrodeposition method was chosen because it is a low-cost, environmentally friendly process that is scalable on large-area substrates. Moreover, by this technique, various nanostructures can be deposited and used without any annealing treatment, which is very interesting for the preparation of photoelectrodes onto plastic substrates.

For improving the electrical performances of DSSCs, another strategy consists to design new sensitizers showing improved optical and electrical properties. In order to replace the classical ruthenium complexes which usually show quite low molar extinction coefficients,²⁵ the research towards dye antenna, inorganic dyes, energy relay dyes, or metal free sensitizers has become very popular. In this work, we also report on the synthesis and characterisation of a new purely organic dye with a high molar extinction coefficient and a wide absorption. The ZnO nanowire-based photoelectrodes

developed in the first part of this work have been combined with this new metal-free organic sensitizer. Using this approach DSSCs employing a iodine based liquid electrolyte or a solid-state hole transporting material have been fabricated and evaluated.

2. Experimental section

2.1. Synthesis of ZnO electrodes

The ZnO electrochemical deposition was carried out in a standard three-electrode electrochemical cell with a volume of 200 mL where a platinum wire was used as a counter electrode and a Saturated Calomel Electrode (SCE) as reference electrode. Two different working electrodes were employed: Glass/In₂O₃.SnO₂ (Glass/ITO) and PolyEthylene Naphthalate/In₂O₃.SnO₂ (PEN/ITO). The sheet resistances of the Glass/ITO and PEN/ITO substrates are 12 Ω/sq and 15 Ω/sq, respectively. The active surface area of the working electrode was fixed at 0.7 cm². The ZnO thin films (buffer layers) and ZnO nanowires were deposited at a constant potential ($E = -1.0$ V vs SCE). ZnO buffer layer electrodeposition on Glass/ITO substrate was performed from an electrolyte containing 5 mmol.L⁻¹ ZnCl₂ and 0.1 mol.L⁻¹ KCl, whereas for the electrodeposition on flexible (PEN/ITO) substrates the electrolyte composition was: [ZnCl₂] = 3.75 mmol.L⁻¹ and [KCl] = 0.1 mol.L⁻¹. ZnO nanowires were electrodeposited on both types of substrates from an electrolyte with equal composition: 0.5 mmol.L⁻¹ ZnCl₂ and 0.1 mol.L⁻¹ KCl. The used chemicals were purchased from Fluka (ZnCl₂, 97.0% and KCl, 99.5%), were of analytical reagent grade, and were used without further purification. For all experiments the electrolytes were saturated by intensive molecular oxygen bubbling for 1 hour prior ZnO electrodeposition and maintained at low pressure during the process. The buffer layers were deposited at 60°C and ZnO nanowires at 80°C. The layer thickness is controlled by passed charge density (Q) and ZnO thin films were deposited with 0.6 C.cm⁻² and 0.4 C.cm⁻² for Glass/ITO and PEN/ITO, respectively. ZnO nanowires were deposited with Q = 10 C.cm⁻² when Glass/ITO working electrode was used and 2 C.cm⁻² for the flexible PEN/ITO substrate.

2.2. Characterization techniques

The surface morphology of the thin films was studied by Scanning Electron Microscopy (SEM), Zeiss ULTRA 55. X-ray diffraction data were recorded on a Panalytical X'Pert MPD X-ray diffractometer using the Co K_α radiation 1.7889 Å wavelength. The absorption spectra of ZnO photoelectrodes were measured between 300 - 900 nm at room temperature. The transmittance is measured in the visible spectral wave range at room temperature with a Perkin Elmer Lambda 35 spectrometer. Current density-voltage (J-V) characteristics were recorded in air using a Keithley 2400 source-measure unit under simulated solar emission (Atlas Solarconstant 575PV). The spectral mismatch between the emission of the solar simulator and the global AM 1.5 G solar spectrum (ASTM G173-03) was corrected using a mismatch factor and the solar simulator irradiance was adjusted accordingly using a certified silicon reference cell in order to achieve an equivalent AM 1.5 G irradiance of one sun (100 mW.cm⁻²) on the test cells.

UV-vis absorption spectra were recorded in solution on a Perkin-Elmer Lambda 2 spectrometer (wavelength range: 180 - 820 nm; resolution: 2 nm) and were confirmed during the SEC analyses using a diode array UV-VIS spectrometer. The fluorescence spectra were recorded on a HITACHI F4500 spectrophotometer. Electrochemical studies of the dye were carried out in a one compartment, three-electrode electrochemical cell equipped with a flat platinum working electrode (7 mm²), a Pt wire counter electrode, and a Ag wire

pseudo-reference electrode, whose potential was checked using the Fc/Fc⁺ couple as an internal standard. The electrolyte consisted of 0.1 mol.L⁻¹ tetrabutylammonium hexafluorophosphate (Bu₄NPF₆) solution in acetonitrile. The experiments were carried out in a glove box filled with argon.

2.3. Synthesis of PK1 Organic Dye.

Reagents and chemicals were purchased from Aldrich, Acros or TCI and used as received, except for THF which was distilled over sodium-benzophenone prior to use. Thin layer chromatography was performed on silica gel-coated aluminium plates with a particle size of 2 - 25 μm and a pore size of 60 Å. Merck 60 (70 - 230 mesh) silica was used for flash chromatography. All synthesised products were identified by ¹H and ¹³C NMR spectroscopy, as well as by elemental analysis or HRMS. NMR spectra were recorded in chloroform-*d*, containing tetramethylsilane (TMS) as internal standard, on a Bruker AC200 spectrometer. Elemental analyses (C, H, N, and S) were carried out by CRMPO at the university of Rennes 1 (France).

4,7-bis(4-octylthiophen-2-yl)benzo[c][1,2,5]thiadiazole (1). In a two necks flask under argon, 2150 mg (6.97 mmol, 2.2 eq) of 5,5-dimethyl-2-(4-octylthien-2-yl)[1,3,2]dioxaborinane and 937 mg (3.18 mmol, 1 eq) of dibromo-benzo[c][1,2,5]thiadiazole were dissolved in a mixture of 50 mL of THF, 10 mL of water and 15 mL of toluene. The mixture was stirred under argon for 20 minutes and then 1500 mg (6.45 mmol, 2.4 eq) of K₂CO₃ and 185 mg (5% molar) of Pd(PPh₃)₄ were added. The solution was stirred 14 hours at 75°C. The reaction mixture was then poured on water (100 mL), and extracted with 2 × 100 mL of diethyl ether. The organic phase was washed with 2 × 100 mL of NaCl saturated aqueous solution and dried over Na₂SO₄. After evaporation of the solvent, the crude product was purified by silica gel column chromatography with hexane/ CH₂Cl₂ (4:1 v/v) as eluent to afford, compound 1 as an orange powder (1300 mg, 77.5%). ¹H NMR (200 MHz, CDCl₃, δ): 7.97 (s, 2H), 7.82 (s, 2H), 7.05 (s, 2H), 2.70 (t, 4H), 1.71 (m, 4H), 1.30 (m, 20H), 0.90 (t, 6H). All other analytical data were similar to those reported in reference [26]

4,7-bis(5-bromo-4-octylthiophen-2-yl)benzo[c][1,2,5]thiadiazole (2). In a two necks flask under argon, 2000 mg (3.83 mmol, 1 eq) of (1) were dissolved in 50 mL of CHCl₃. Then, a solution of 177.9 mg (1.00 mmol, 2.2 eq) of N-bromosuccinimide previously dissolved in 50 mL of CHCl₃ was added drop wise at room temperature over 30 minutes. The mixture was stirred during 24 hours. The solution was poured in HCl 1 mol.L⁻¹ aqueous solution then extracted with 2 × 100 mL of diethyl ether. Organic phase was washed with 2 × 100 mL of NaCl saturated aqueous solution and dried over Na₂SO₄. After evaporation of the solvent, the crude product was purified by silica gel column chromatography with hexane as eluent to afford, compound 1 as a red powder (2.60 g, 99%). ¹H NMR (200 MHz, CDCl₃, δ): 7.77 (s, 2H), 7.75 (s, 2H), 2.64 (t, 4H, J = 7.2 Hz), 1.73-1.59 (m, 4H), 1.43-1.26 (m, 20H), 0.88 (t, 6H, J = 6.5Hz). All other analytical data were similar to those reported in reference [26]

4,7-bis(3-octyl-2,2'-bithiophen-5-yl)benzo[c][1,2,5]thiadiazole (3). A mixture of 4,7-bis(5-bromo-4-octylthiophen-2-yl)benzo[c][1,2,5]thiadiazole (1) (217 mg, 0.32 mmol), 5,5-dimethyl-2-(thiophen-2-yl)-1,3,2-dioxaborinane (1.49 g, 0.76 mmol), and Pd(PPh₃)₄ (15 mg, 4% molar), K₃PO₄ (155 mg, 0.76 mmol) dissolved in 30 mL of DMF was refluxed overnight. The mixture was then allowed to cool to room temperature before addition of 1 mol.L⁻¹ HCl and extracted with diethyl ether. The organic layer was dried over Na₂SO₄ and the solvent was evaporated. The crude

product was purified by silica gel column chromatography with hexane/chloroform (4:1 v/v) as eluent to afford 4,7-bis(3-octyl-2,2'-bithiophen-5-yl)benzo[c][1,2,5]thiadiazole (3) as red powder. (50 mg, 23 %). ¹H NMR (200 MHz, CDCl₃, δ): 7.99 (s, 2H), 7.83 (s, 2H), 7.36 (dd, *J*₁ = 5 Hz, *J*₂ = 1.2 Hz, 2H); 7.25 (dd, *J*₁ = 3.6 Hz, *J*₂ = 1.2 Hz, 2H; Ar H), 7.13 (dd, *J*₁ = 5.2 Hz, *J*₂ = 3.6 Hz, 2H; Ar H), 2.85 (t, *J* = 7.2 Hz, 4H; CH₂), 1.83-1.55 (m, 4H; CH₂), 1.47-1.21 (m, 20H; CH₂), 0.88 (t, 6H, *J* = 6.6 Hz; CH₃). ¹³C NMR (200 MHz, CDCl₃, δ): 152.49, 140.48, 136.86, 136.01, 132.31, 130.54, 127.48, 126.01, 125.54, 125.39, 31.88, 30.66, 29.62, 29.44, 29.29, 22.68, 14.14. Elemental analysis for C₃₈H₄₄N₂S₅ (Calc.): C, 66.23; H, 6.44; N, 4.07; S, 23.27; Found: C, 65.53; H, 6.64; N, 3.88; S, 22.12

4,7-bis(5'-bromo-3-octyl-2,2'-bithiophen-5-yl)benzo[c][1,2,5]thiadiazole (4). 4,7-bis(3-octyl-2,2'-bithiophen-5-yl)benzo[c][1,2,5]thiadiazole (3) (267 mg, 0.39 mmol) was dissolved in 10 mL of chloroform. N-bromosuccinimide (145 mg, 0.81 mmol) dissolved in 10 mL of chloroform was then added dropwise at room temperature. After stirring for overnight at room temperature, the resulting mixture was poured into 20 mL of water, and then extracted with dichloromethane. After solvent removal, the crude product was purified by silica gel column chromatography with cyclohexane as eluent to afford the expected product as violet powder. (312 mg, 95 %). ¹H NMR (200 MHz, CDCl₃, δ): 7.95 (s, 2H), 7.81 (s, 2H), 7.05 (d, *J* = 3.8 Hz, 2H), 6.97 (d, *J* = 3.8 Hz, 2H; Ar H), 2.79 (t, *J* = 7.8 Hz, 4H; CH₂), 1.78-1.64 (m, 4H; CH₂), 1.21 (m, 20H; CH₂), 0.89 (t, 6H, *J* = 6.6 Hz; CH₃). Elemental analysis for C₃₈H₄₂Br₂N₂S₅ (Calc): C, 53.89; H, 5.00; N, 3.31; S, 18.93. Found: C, 53.67; H, 5.08; N, 3.29; S, 18.92.

4-(5'-(7-(5'-bromo-3-octyl-[2,2'-bithiophen]-5-yl)benzo[c][1,2,5]thiadiazol-4-yl)-3'-octyl-[2,2'-bithiophen]-5-yl)-N,N'-diphenylaniline (5). A mixture of (4) (0.59 mmol, 1 eq), 245 mg (3 eq) of K₂CO₃ and 35 mg (5% molar) of Pd(PPh₃)₄ dissolved in 30 mL of THF and 5 mL of water was degassed under stirring and flushed with argon. Then the mixture was heated at 60°C during 30 minutes and 190 mg (0.53 mmol, 0.9 eq) of 4-(diphenylamino)phenylboronic acid solubilised in 20 mL of THF were added. The reaction mixture was refluxed for 14 hours at 75°C. After usual work up and extraction with diethyl ether, the organic phase was washed with 2 × 100 mL saturated aqueous NaCl solution. The organic layer was dried over Na₂SO₄ and the solvent was evaporated. The crude product was purified by silica gel column chromatography with hexane/CHCl₃: 8/2 to afford the expected product (244 mg, 41%). ¹H NMR (200 MHz, CDCl₃, δ): 7.99 (s, 1H), 7.95 (s, 1H), 7.82 (s, 2H), 7.50 (d, *J* = 8.7 Hz, 2H), 7.30 (d, *J* = 8.1 Hz, 2H), 7.28 (s, 1H), 7.26-7.04 (m, 11H), 6.98 (d, *J* = 3.9 Hz, 2H), 2.88 (t, *J* = 7.8 Hz, 2H), 2.80 (t, *J* = 7.8 Hz, 2H), 1.80-1.60 (m, 4H), 1.50-1.20 (m, 20H), 0.95-0.75 (m, 6H). ¹³C NMR (200 MHz, CDCl₃, δ): 152.8, 147.8, 147.8, 144.5, 141.3, 140.7, 138.0, 137.8, 136.9, 135.0, 133.2, 131.6, 131.2, 130.7, 130.0, 129.7, 128.4, 127.2, 126.8, 126.5, 126.0, 125.7, 125.4, 125.4, 125.0, 124.0, 123.6, 123.0, 112.5, 32.3, 31.0, 30.1, 30.0, 29.9, 29.7, 23.1, 14.6 (2CH₃).

4-(5'-(7-(5'-(4-(diphenylamino)phenyl)-3-octyl-[2,2'-bithiophen]-5-yl)benzo[c][1,2,5]thiadiazol-4-yl)-3'-octyl-[2,2'-bithiophen]-5-yl)benzaldehyde (6). A mixture of (5) 240 mg (0.237 mmol, 1 eq), and 53.4 mg (0.356 mmol, 1.5 eq) of 4-formylphenylboronic acid and 98 mg (3 eq) of K₂CO₃ were dissolved 2.5 mL of water and 25 mL of distilled THF. Then the mixture was heated at 60°C during 30 minutes and 13.7 mg (5% molar) of Pd(PPh₃)₄ were added. The mixture was stirred at 75°C during 14 hours. After usual work up and extraction with diethyl ether, the organic phase was washed with 2 × 100 mL saturated aqueous NaCl solution. The

organic layer was dried over Na₂SO₄ and the solvent was evaporated. The crude product was purified by silica gel column chromatography with cyclohexane/CH₂Cl₂: 6/4 to afford the expected product (240 mg, 97%). ¹H NMR (200 MHz, CDCl₃, δ): 9.84 (s, 1H), 7.86-7.65 (m, 6H), 7.37 (m, 4H), 7.35-6.91 (m, 16H), 2.72 (m, 4H), 1.63 (m, 4H), 1.48-1.21 (m, 20H), 0.77 (t, 6H). ¹³C NMR (200 MHz, CDCl₃, δ): 191.2 (C=O), 152.3, 147.3, 147.2, 144.0, 141.8, 140.9, 140.2, 139.6, 137.8, 137.3, 136.3, 134.8, 134.4, 132.7, 131.7, 130.7, 130.5, 130.4, 130.4, 129.2, 127.8, 126.8, 126.7, 126.3, 125.4, 125.4, 125.4, 125.1, 124.8, 124.4, 123.4, 123.0, 122.4, 118.5, 31.8, 30.4, 30.4, 29.5, 29.3, 29.2, 22.6, 14.0 (CH₃).

2-cyano-3-(4-(5'-(7-(5'-(4-(diphenylamino)phenyl)-3-octyl-[2,2'-bithiophen]-5-yl)benzo[c][1,2,5]thiadiazol-4-yl)-3'-octyl-[2,2'-bithiophen]-5-yl)phenyl)acrylic acid : PK1. In a two necks flask, 210 mg (0.20 mmol) of (6) and 26 mg (0.30 mmol, 1.5 eq) of cyanoacrylic acid were dissolved in 30 mL of CH₃CN under argon. Few drops of pyridine were added and the reaction mixture was refluxed during 2 hours. Then the acetonitrile was evaporated under vacuum and the crude product was dissolved in chloroform. The solution was washed with HCl 2 mol.L⁻¹ aqueous solution and then with water. The organic layer was dried over Na₂SO₄ and the solvent was evaporated. The crude product was purified by silica gel column chromatography with THF/MeOH: 9/1 to afford the expected product as a dark purple powder (78%). ¹H NMR (200 MHz, CDCl₃, δ) 7.97 (d, 2H), 7.84 (s, 2H), 7.49 (dt, 2H), 7.31-7.17 (m, 7H), 7.12-6.97 (m, 9H), 2.82 (m, 4H), 1.70 (m, 4H), 1.48-1.21 (m, 20H), 0.86 (t, 6H). H MRS [M-H]⁻(C₆₆H₆₁N₄O₂S₅) : 1101.33981, m/z calculated 1101.33981, m/z found: 1101.34040.

2.4. Fabrication of Dye-Sensitized Solar Cells

ZnO electrodes are immersed in diluted solution of PK1/chenodeoxycholic acid = 1/10 (0.2 mmol.L⁻¹ of PK1 in a CH₃Cl/ethanol = 1/1 solution). The dye-sensitized ZnO electrodes are then rinsed and infiltrated by a commercial liquid electrolyte from Dyesol (EL HSE) or by the molecular hole conductor 2,2',7,7'-tetrakis(N,N-dip-methoxyphenyl-amine)-9,9'-spirobifluorene (spiro-OMeTAD, Merck KGaA) from spin-coating, using conventional procedures reported elsewhere [30d]. Gold top electrodes were finally evaporated under vacuum (10⁻⁶ mbar) using shadow masks that define two active areas per substrates (0.18 cm² each).

3. Results and discussion

3.1. Preparation and characterisation of the ZnO photoelectrodes

In this work ZnO was deposited using the molecular oxygen reduction method pioneered by Lincot and co-workers.²⁷ The electrochemical molecular oxygen reduction leads to the generation of hydroxide ions (OH⁻), which with Zn²⁺ ions present in the electrolyte form the unstable zinc hydroxide, and owing to the supersaturation and the chemical precipitation, ZnO is obtained in the vicinity of the electrode. ZnO photoelectrodes used for the fabrication of DSSCs were prepared by a two-steps process. In the first step a compact ZnO thin film is deposited onto the conducting ITO layer of the working electrode. In the second step ZnO nanowires are electrochemically grown on the buffer layer formed in the first step. The deposition conditions allowing the formation of dense buffer layer were optimized for each type of substrate. It has been found that for the deposition of continuous defect free ZnO thin films the optimal bath temperature should be 60°C for both used substrates, whereas ZnCl₂ precursor concentration in the electrolyte should be different. For example, the buffer layer onto Glass/ITO

substrate is deposited from a solution containing higher ZnCl_2 concentration (5 mmol.L^{-1}) than that used for the flexible (PEN/ITO) substrate (3.75 mmol.L^{-1}). The surface morphology of the deposited buffer layers is smooth (Fig. 1a and b) and from the SEM images it was estimated that the layer thickness is about 150 nm. One can observe that the ZnO buffer layer deposited on the Glass/ITO substrate looks denser than that grown on the flexible PEN/ITO substrate.

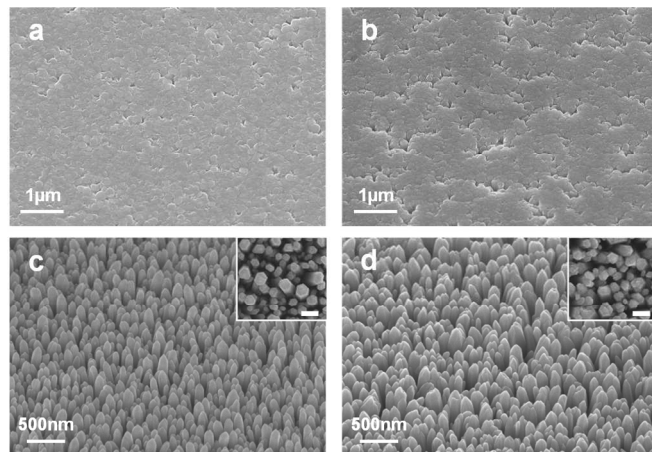


Fig. 1 SEM images of the electrodeposited ZnO buffer layer on: a) Glass/ITO and b) PEN/ITO. ZnO nanowires electrodeposited: c) on buffer layer from (a) and d) on buffer layer from (b). The insets in (c) and (d) are top view of these images with 200 nm scale bar

In the second step ZnO nanowires have been grown on the ZnO thin films. In order to obtain ZnO in nanowire form it is necessary to lower the Zn^{2+} concentration in the electrolyte and to increase the bath temperature to 80°C .²⁸ The evolution of the mean values of the diameter and length of the nanowires is known to depend strongly on the KCl concentration.^{28d} For the fabrication of DSSCs based on liquid electrolytes long ZnO nanowires would be of interest since they demonstrate large surface area.²⁰ However, in this work, the length of the nanowires was voluntarily limited to about 650 nm in order to insure later a good infiltration of the hole conductor (spiro-OMeTAD) into the ZnO matrix during the fabrication of the solid-state DSSCs. We have found that a charge density of 10 C cm^{-2} was needed to grow nanowires of 650 nm on Glass/ITO substrate. In contrary, for the flexible substrate (PEN/ITO), a much lower charge density (2 C.cm^{-2}) was needed to obtain nanowires with the same length. This result could be due to different buffer layer conductivity and density. From the SEM images depicted in Fig. 1c and 1d one can see that the electrodeposited nanowire arrays are very dense on both substrates and their diameter is between 60 and 150 nm.

The XRD patterns of ZnO thin films and nanowires are shown in Fig. 2. All diffraction peaks can be indexed from ZnO wurtzite structure (JCPDS card No. 36-1451) and PEN substrate, and peaks corresponding to ITO are not observed. The higher intensity of 002 peak (for both thin film and thin film with nanowires) confirms the preferential growth along the c-axis of the ZnO nanostructures.

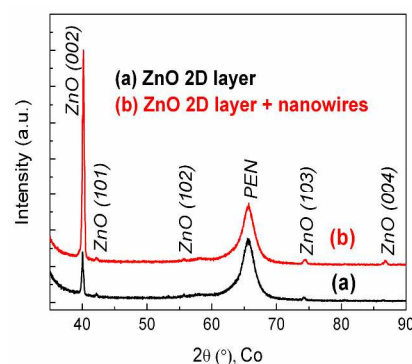


Fig. 2 XRD patterns of: (a) ZnO 2D layer and (b) ZnO 2D layer and ZnO nanowires deposited on PEN/ITO substrates. The indexed peaks correspond to ZnO wurtzite phase and PEN

The as-prepared ZnO 2D layer and nanowires are nearly 85% transparent in the visible spectral wave range, similar to the bare Glass/ITO and PEN/ITO substrate (Fig. 3).

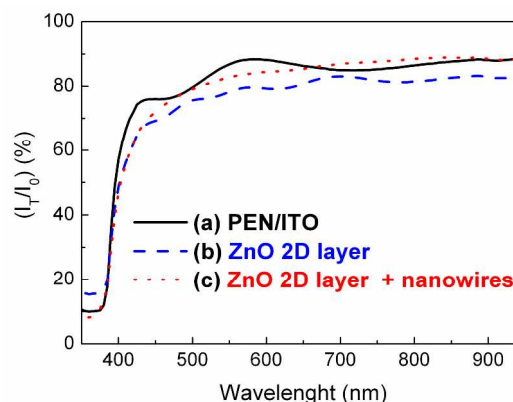
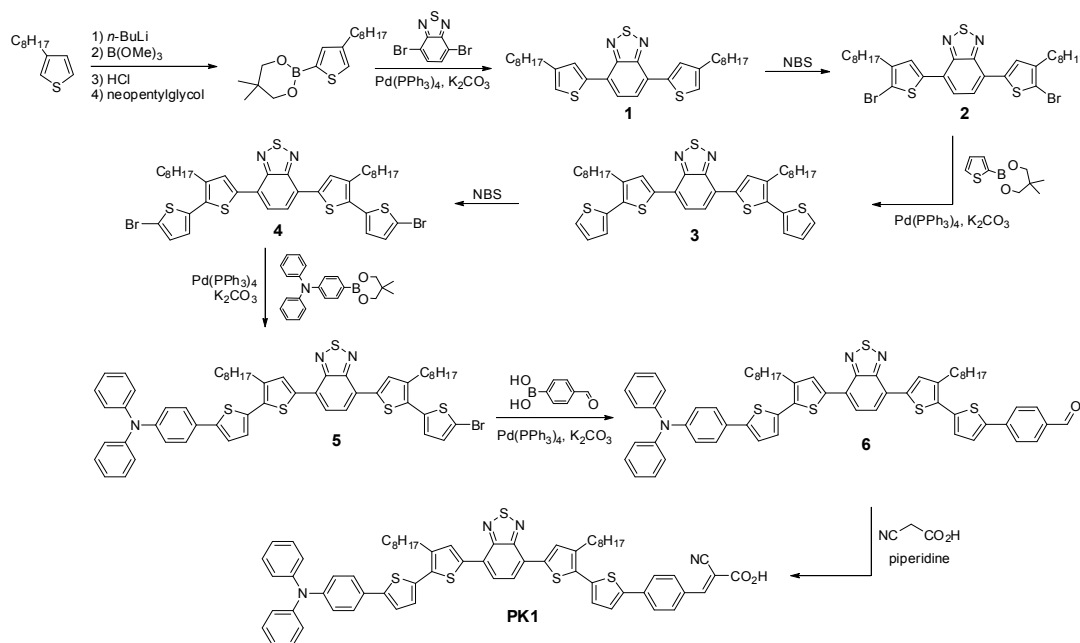


Fig. 3 Transmission spectra of: (a) PEN/ITO bare substrate; (b) ZnO 2D layer and (c) ZnO 2D layer and nanowires

3.2. Preparation and characterization of the organic dye

Sensitizing dyes are crucial elements in DSSCs. Despite of the fact that most of the high performances DSSCs have been fabricated using ruthenium-based complexes that show broad absorption spectra,²⁹ these dyes unfortunately have low molar extinction coefficients ($< 25000 \text{ mol}^{-1}.\text{cm}^{-1}$).³⁰ The use of highly absorbing dyes presenting higher molar extinction was reported to be compatible with thinner porous electrodes.³⁰ One possible strategy to obtain organic dyes with improved optical properties is to combine electron-withdrawing groups with electron releasing groups. The absorption spectra of these materials better match the solar emission spectrum mainly because an intra-molecular charge transfer (ICT) process between electron donor and electron acceptor segments occurs, giving rise to strong absorption bands especially in the visible region. For this reason, we decided to design and synthesize a new organic dye based on benzothiadiazole and thiophene units, hoping that the combination of these building blocks would lead to a molecule showing a wide absorption spectrum and a high molar extinction coefficient. The synthetic strategy that has been developed to access to PK1 dye is depicted in **Scheme 1**.



Scheme 1 Synthetic route to PK1

Starting from 2,5-dibromobenzothiadiazole and 5,5-dimethyl-2-(4-octylthien-2-yl)[1,3,2]dioxaborinane,³¹ the symmetric compound (**1**) was obtained by Palladium-catalysed cross-coupling reaction according to Suzuki conditions. This compound was then converted to dibrominated derivative (**2**) by bromination with NBS. It should be pointed out that this reaction should be carried out at 0°C in order to avoid the formation of tris-brominated side products that are produced at higher temperature.

From this compound, a second Suzuki coupling reaction involving two equivalent of 5,5-dimethyl-2-(thien-2-yl)[1,3,2]dioxaborinane afforded the symmetric molecule (**3**) which was subsequently dibrominated using the same conditions as previously described. Electron donor triarylamine moiety was attached on one side of this pi-conjugated bridge via Suzuki coupling reaction to give compound (**5**) followed by the attachment of the phenyl-carbonyl unit under the same conditions. In the last step, the precursor (**6**) was then converted to the corresponding sensitizer **PK1** by Knoevenagel condensation using cyanoacetic acid. This reaction was carried out through refluxing acetonitrile in the presence of pyridine.

The electronic and optical properties of the new dye were investigated by UV-Visible spectroscopy and cyclic voltammetry (Fig. 4). The benzothiadiazole-containing dyes usually show two absorption peaks caused by the presence of this additional chromophores.³² The first peak is located at the frontier between the UV and the visible parts of the spectrum located at $\lambda = 387$ nm with $\epsilon = 36700 \text{ mol}^{-1} \cdot \text{cm}^{-1}$, corresponds to the $\pi-\pi^*$ transition of the different π -conjugated aromatic rings being in conjugation. The longer wavelength band, *i.e.* the one observed in the visible part of the spectrum and located at $\lambda = 536$ nm with $\epsilon = 36400 \text{ mol}^{-1} \cdot \text{cm}^{-1}$,

can be ascribed to an ICT that occurs between the electron rich oligo(thiophene) segments and the central benzothiadiazole core. Interestingly the absorption edge of this new dye is close to 700 nm in solution.

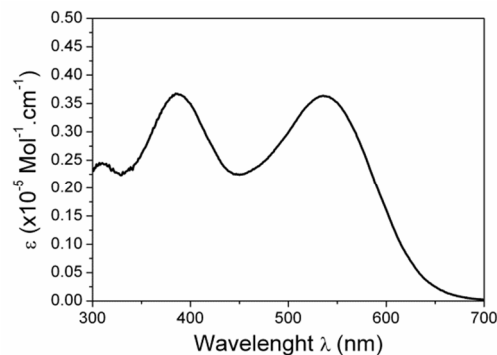


Fig. 4 UV-Visible absorption spectrum of **PK1** in chloroform solution ($10^{-5} \text{ mol} \cdot \text{L}^{-1}$)

From the cyclic voltammetry measurements (see ESI), HOMO and LUMO energy levels were estimated. The experimental value for the HOMO energy level was -5.00 eV whereas the LUMO energy level was found lying at -3.25 eV. It is therefore clear that the LUMO energy of the sensitizer is appropriate for efficient electron injection in the conduction band of various oxides such as ZnO or TiO₂. LUMO and HOMO level electron-density distributions of the dye were investigated using B3LYP (see ESI). We found that the combination of benzothiadiazole with bithiophene units, not only guarantee a good electronic conjugation, but it also ensures enough

distance between the HOMO and LUMO to avoid charge recombination between TiO₂ conduction band electrons and the oxidized dyes.³³

3.3. Device fabrication and characterization

After the electrochemical deposition of ZnO nanowires, chemical synthesis and the complete physico-chemical characterization of the new dye, we pursued our study by testing the applicability of these materials for photovoltaic energy conversion. Solid-state cells were prepared according to a modified procedure compared to a procedure fully described in previous reports.³⁴ The ZnO nanowires were photosensitized by a solution containing the PK1 organic dye (0.02 mol.L⁻¹) and chenodeoxycholic acid (0.2 mol.L⁻¹). After 14 hours in the solution, we observed the coloration of the ZnO layer. The SEM investigation of the nanowires confirmed that no etching phenomenon or other alteration of the substrate by the organic dye was provoked during the photosensitization. This result is very important because ZnO electrodes due to its amphoteric nature can present a poor chemical stability in the presence of acidic dyes and etching processes have been reported with ruthenium-based dye.^{35,36} A similar result has been reported with the indoline dye D149 and ZnO commercial powder.¹² After the grafting of the compound, we have measured the absorption spectra of the sensitized ZnO photoelectrodes (Fig. 5). A strong absorption band attributed to ZnO is seen between 300 - 400 nm in the UV domain. In the case of ZnO nanowires tainted with PK1, an additional large absorption band corresponding to the contribution of the dye appears in the visible region between 400 - 700 nm.

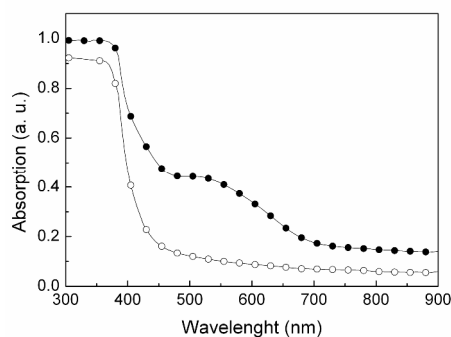


Fig. 5 Optical absorption spectra of bare ZnO nanowires (○) and photosensitized ZnO nanowires with PK1 (●)

In the next step the photosensitized ZnO nanowire array was filled using solid electrolyte using spiro-OMeTAD. After deposition by spin-coating of the spiro-OMeTAD, the overlayer thickness, and the depth of penetration between the nanowires were accurately evaluated from the cross-sectional SEM images, as depicted in Fig. 6. Indeed, the proper device operation requires an intimate contact of

the ZnO-dye with the hole transporting material in order to ensure efficient hole transfer and hopping to the top gold anode.

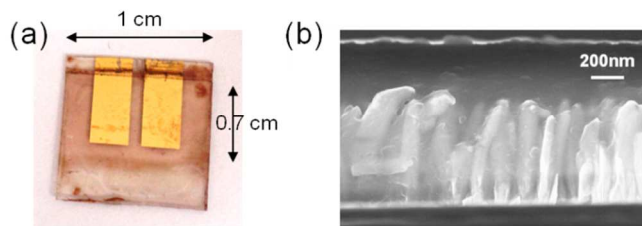


Fig. 6 (a) Top view of the device fabricated on flexible substrate, (b) cross-sectional SEM image of a full device. The cell architecture comprises from the bottom to the top: ITO/ZnO 2D layer/ZnO nanowires/PK1/spiro-OMeTAD/Au top electrode

One can observe that the spiro-OMeTAD penetrates between the nanowires and reaches the bottom buffer layer. It can also be seen that an overlayer of about 250 nm thickness is formed over the nanowire array, preventing a direct contact of the evaporated gold top electrode with the nanowires.

Three different DSSCs based on ZnO nanowires and PK1 were fabricated. Sample 01 (SC01) and Sample 02 (SC02) were prepared with ZnO nanowires deposited on Glass/ITO and filled with liquid electrolyte (I⁻/I₃⁻ in acetonitrile) and spiro-OMeTAD as hole conductor, respectively. Sample 03 (SC03) is a flexible solid DSSC, where a PEN/ITO/ZnO photoelectrode and spiro-OMeTAD are used. The performances were evaluated by recording J-V curves under normalized illumination (Fig. 7). Table 1 summarizes the results and presents the different key photovoltaic parameters: short-circuit current density (J_{SC}), open-circuit voltage (V_{OC}), fill factor (FF) and power conversion efficiency (PCE).

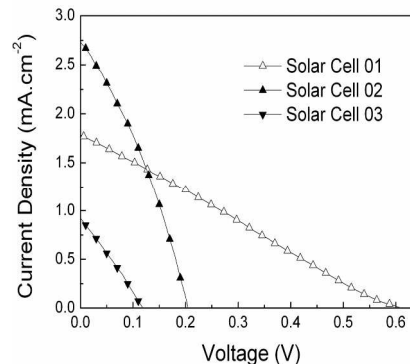


Fig. 7 Current-voltage characteristics of DSSC devices. Measurements are performed under 100 mW.cm⁻², AM 1.5G simulated solar spectrum

Table 1 Photovoltaic parameters under simulated solar emission (100 mW.cm⁻², AM 1.5 G) of the different devices investigated in this work as a function of substrate, electrolyte, charge density (Q) and ZnO nanowires length (NW length): short-circuit current density (J_{SC}); open-circuit voltage (V_{OC}); fill factor (FF); power conversion efficiency (PCE). (a) Reference²⁰, (b) reference³⁷

Samples	Substrate	Electrolyte	Q (C.cm ⁻²)	NW length (μm)	J _{SC} (mA.cm ⁻²)	V _{OC} (mV)	FF (%)	PCE (%)
SC01	Glass/ITO	Liquid electrolyte	10	0.65	1.78	606	25	0.27
SC02	Glass/ITO	Spiro-OMeTAD	10	0.65	2.74	200	35	0.18
SC03	PEN/ITO	Spiro-OMeTAD	2	0.65	0.92	120	29	0.03
Pauporté et al. ^(a)	Glass/FTO	Liquid electrolyte	14	3.00	2.52	530	37	0.49
Plank et al. ^(b)	Glass/FTO	Spiro-OMeTAD	-	0.65	1.05	570	42	0.25

The power conversion efficiency (PCE) of SC01 is 0.27% associated to a low FF and J_{SC} . The value of the open-circuit voltage is in good agreement with the values reported previously for ZnO solar cell.²⁰ The lower open-circuit voltage can be explained by the charge recombination process that is slightly accelerated in ZnO compared to TiO₂ electrodes in reverse bias conditions.¹² Pauporté et al. reported a PCE of 0.49% for a device combining electrodeposited ZnO nanowires, organic dye (D149) and liquid electrolyte. The lower performances of SC01 could be related to the shorter nanowires, 650 nm in our case compared to 3 μ m for the cells fabricated by Pauporté and co-workers.²⁰ The small length of nanowires is responsible for a lower dye loading and the weaker photon absorption. Therefore the J_{SC} and FF of SC01 are lower than those of Pauporté device. Nevertheless the J_{SC} value of SC01 is relatively large ($J_{SC} = 1.78 \text{ mA}\cdot\text{cm}^{-2}$) considering the short length of the nanowires. Although the nanowires of SC01 are 4.6 times shorter than those reported in reference,²⁰ we only observe a 29% J_{SC} decrease. This result can be attributed to better light harvesting properties of the dye. The second device (SC02) was built with the same type of photoelectrode than SC01 but in this sample, spiro-OMeTAD replaces the liquid electrolyte. An important literature exists on TiO₂-based solid-state DSSCs, but only few examples of ZnO solid-DSSCs are reported.³⁷ For example, SC02 is the first solid DSSC prepared with electrodeposited ZnO nanowires. The most efficient ZnO nanowires solid DSSC has been obtained by Plank et al. by sputter deposition process and hydrothermal growth method.³⁷ The device architecture is similar to the one employed to SC02 (Glass/FTO/dense ZnO/ZnO nanowires/organic dye (D102) and spiro-OMeTAD) and the length of the nanowires is similar to one reported in our work (650 nm). The efficiency of our SC02 is close to the best value reported by Plank et al.,³⁷ 0.18% versus 0.25%. However the J_{SC} value of SC02 is higher, 2.74 $\text{mA}\cdot\text{cm}^{-2}$ compared to 1.05 $\text{mA}\cdot\text{cm}^{-2}$. A better photon absorption by the organic dye can explain the improvement of the J_{sc} despite of a low FF. Based on these promising preliminary results we consider that the density of the blocking layer and the thickness of the spiro-OMeTAD over layer should be optimized in order to improve further the device efficiency. This work is actually in progress.

Finally, the third solar cell (SC03) which we have investigated in this study is the first example of flexible solid-DSSC with an electrodeposited ZnO photoelectrode. It is identical to those prepared on Glass/ITO substrate and the parameters of the spin-coating of spiro-OMeTAD are also the same. This new device has shown an efficiency of 0.03%, a value which is lower than the PCE of SC02 (0.18%). This poor efficiency could be due to different reasons. One possibility is that the ZnO buffer layer of SC03 is less dense than the buffer layer of SC02. Consequently the charge recombination process induced by some direct contacts between the ITO electrode and the hole transporter can be more important for SC03 than for SC02. Indeed, we have found that the electrochemical deposition of dense ZnO films on flexible substrate is more difficult than on Glass/ITO. The PEN/ITO is more sensitive to the slightly elevated temperature (60 and 80°C) of the electrochemical deposition than Glass/ITO. We observed that longer deposition times lead to slightly damage the ITO layer. That is why the deposition of ZnO nanowires onto PEN/ITO substrate was limited to $Q \leq 5 \text{ C}\cdot\text{cm}^{-2}$. Larger passed charge densities (up to 10 $\text{C}\cdot\text{cm}^{-2}$) were found to deteriorate the ITO layer.

4. Conclusions

In summary, we have reported a new promising electrodeposited ZnO nanowire photoelectrode for solid-state DSSCs. In parallel a new organic dye, PK1, showing intense absorption across the visible

range of the solar emission spectrum has been developed and efficiently employed for the sensitization of ZnO nanowires. Despite limited conversion efficiencies, we consider that electrochemically deposited ZnO nanowires remain interesting for the fabrication of new device architectures, especially on plastic substrates. Taking into account that longer nanowires show larger specific surface to attach the dyes, higher efficiencies could be expected which requires the development of specific infiltration methods of the hole transporting material into the nanostructured electrode. These preliminary results demonstrate the possibility to realize original structures on flexible substrates. Work is currently under progress to validate the potential of PK1 dye for the sensitization of other metal oxides such as TiO₂ or Zn₂SnO₄ and further investigations are under progress in order to optimize the different experimental parameters in order to demonstrate efficient ZnO-based solid-state DSSC processed at low temperature.

Acknowledgements

This work was partially funded by the Programme Interdisciplinaire Energie (CNRS), Colhybride research programs and the CEA Chimtronique research program PV-ZnO-H (2011). H. Muguerra gratefully acknowledges Commissariat à l'Énergie Atomique et aux Énergies Alternatives (CEA) and Eurotalents program for postdoctoral fellowship. The authors also thank Laurent Terrier from LMGP laboratory of INP Grenoble for his help for transmittance measurements.

Notes and references

- ^a INAC/SPRAM UMR 5819 CEA-CNRS-Univ. J. Fourier-Grenoble, LEMOH, 17 Rue des Martyrs, 38054 Grenoble Cedex 9, France. E-mail: renaud.demadrille@cea.fr; Fax: +33 438785145; Tel: +33 438784484
- ^b CEA-Leti, MINATEC Campus, 17 rue des Martyrs, 38054 Grenoble Cedex 9, France.
- ^c XLIM UMR 7252, Université de Limoges/CNRS, 123 Avenue Albert Thomas, 87060 Limoges Cedex, France. E-mail: johann.boucle@unilim.fr; Fax: +33 555457649; Tel: +33 587506762
- 1 A. Hagfeldt, G. Boschloo, L. Sun, L. Kloo and H. Pettersson, *Chem. Rev.*, 2010, **110** (11), 6595.
- 2 M. Grätzel, *Nature*, 2003, **421**, 586.
- 3 B. O'Regan and M. Grätzel, *Nature*, 1991, **353**, 737.
- 4 B. E. Hardin, H. J. Snaith and M. D. McGehee, *Nat. Photon.*, 2012, **6**, 162.
- 5 Md. K. Nazeeruddin, E. Baranoff and M. Grätzel, *Solar Energy*, 2011, **85**, 1172.
- 6 A. Yella, H.-W. Lee, H. N. Tsao, C. Yi, A. K. Chandiran, Md. K. Nazeeruddin, E. Wei-Guang Diao, C.-Y. Yeh, S. M. Zakeeruddin and M. Grätzel, *Science*, 2011, **334**, 629.
- 7 A. Kay, M. Grätzel, *Chem. Mater.*, 2002, **14**, 2930; E. Naveen Kumar, R. Jose, P. S. Archana, C. Vijila, M. M. Yusoff and S. Ramakrishna, *Energy Environ. Sci.*, 2012, **5**, 5401; Y. P. Y. P. Ariyasinghe, T. R. C. K. Wijayarathna, I. G. C. K. Kumara, I. P. L. Jayarathna, C. A. Thotawatthage, W. S. S. Gunathilake, G. K. R. Senadeera and V. P. S. Perera, *J. Photochem. Photobiol. A: Chemistry*, 2011, **217**, 249.
- 8 P. Guo, M. A. Aegerter, *Thin Solid Films* 1999, **351**, 290; K. Sayama, H. Sugihara and H. Arakawa, *Chem. Mater.*, 1998, **10**, 3825.
- 9 K. Hara, T. Horiguchi, T. Kinoshita, K. Sayama, H. Sugihara and H. Arakawa, *Sol. Energy Mater. Sol. Cells*, 2000, **64**, 115.
- 10 K. Kakiuchi, E. Hosono and S. Fujihara, *J. Photochem. Photobiol. A: Chem.*, 2006, **179**, 81; K. Keis, E. Magnusson, H. Lindstrom, S. - E. Lindquist, A. Hagfeldt, *Sol. Energy Mater. Sol. Cells* 2002, **73**, 51; N. Memarian, I. Concina, A. Braga, S. M. Rozati, A. Vomiero and G. Sberveglieri, *Angew. Chem.*, 2011, **50**, 12321.
- 11 Y. W. Heo, D. P. Norton, L. C. Tien, Y. Kwon, B. S. Kang, F. Ren, S. J. Pearton and J. R. LaRoche, *Mater. Sci. Eng. R.*, 2004, **47**, 1; C.

- Klingshirn, *Chem. Phys. Chem.*, 2007, **8**, 782; L. Schmidt-Mende and J. L. MacManus-Driscoll, *Today*, 2007, **10**, 40.
- 12 M. Quintana, T. Edvinsson, A. Hagfeldt and G. Boschloo, *J. Phys. Chem. C*, 2007, **111**, 1035; N. O. V. Plank, H. J. Snaith, C. Ducati, J. S. Bendall, L. Schmidt-Mende, M. E. Welland, *Nanotechnology*, 2008, **19**, 465603; R. L. Willis, C. Olson, B. O'Regan, T. Lutz, J. Nelson and J. R. Durrant, *J Phys Chem B*, 2002, **106**, 7605.
- 13 M. Saito and S. Fujihara, *Energy Environ. Sci.*, 2008, **1**, 280.
- 14 S. – B. Ambade, R. – S. Mane, S. – H. Han, S. – H. Lee, M. – M. Sung and O. – S. Joo, *J. Photochem. Photobiol. A*, 2011, **222**, 366-36.
- 15 C. – Y. Lin, Y. – H. Lai, H. – W. Chen, J. – G. Chen, C. – W. Kung, R. Vittal and K. – C. Ho, *Energy Environ. Sci.*, 2011, **4**, 3448.
- 16 M. Law, L. E. Greene, J. C. Johnson, R. Saykally and P. Yang, *Nat. Mater.*, **2005**, **4**, 455.
- 17 C. Xu, J. Wu, U. V. Desai, D. Gao, *J. Am. Chem. Soc.*, **2011**, **133**, 8122.
- 18 W. Chen, Y. Qiu, Y. Zhong, K. S. Wong, S. Yang, *J. Phys. Chem. A*, **2010**, **114**, 3127.
- 19 S. Baruah and J. Dutta, *Sci. Technol. Adv. Mater.*, 2009, **10**, 013001.
- 20 V.-M. Guérin and T. Pauporté, *Energy Environ. Sci.*, **2011**, **4**, 2971.
- 21 N. Memarian, I. Concina, A. Braga, S. M. Rozati, A. Vomiero and G. Sberveglieri, *Angew. Chem.*, **2011**, **50**, 12321.
- 22 Q. F. Zhang, T. R. Chou, B. Russo, S. A. Jenekhe and G. Z. Cao, *Angew. Chem*, **2008**, **47**, 2402.
- 23 E. Galoppini, J. Rochford, H. H. Chen, G. Saraf, Y. C. Lu, A. Hagfeldt and G. J. Boschloo, *Phys. Chem. B*, **2006**, **110**, 16159
- 24 L. - Y. Lin, M. - H. Yeh, C. - P. Lee, C. - Y. Chou, R. Vittal and K. – C. Ho, *Electrochimica Acta* **62**, **2012**, 341; O. Lupan and T. Pauporté, *Journal of Crystal Growth*, **2010**, **312**, 2454; C. Y. Jiang, X. W. Sun, K. W. Tan, G. Q. Lo, A. K. K. Kya and D. L. Kwong, *Applied Physics Letters*, **2008**, **92**, 143101.
- 25 C. - Y. Chen, M Wang, J. – Y. Li, N. Pootrakulchote, L. Alibabaei, C. Ngoc-le, J. – D. Decoppet, J. - H. Tsai, C. Graetzel, C. – G. Wu, S. M. Zakeeruddin and M. Grätzel, *ACS Nano*, **2009**, **3**, 3103.
- 26 S. K. Lee, S. Cho, M. Tong, J. H. Seo and A. J. Heeger, *J. Polym. Science Part A: Polym. Chem.*, **2011**, **49**, 1821.
- 27 a) S. Peulon, D. Lincot, *Adv. Mater.*, 1996, **8**, 166; b) S. Peulon and D. Lincot, *J. Electrochem. Soc.*, 1998, **145**, 864.
- 28 a) R. Salazar, C. Lévy-Clément and V. Ivanova, *Electrochim. Acta*, 2012, **78**, 547; b) S. Sanchez, C. Lévy-Clément and V. Ivanova, *J. Electrochem. Soc.*, 2012, **159**, D705; c) S. Sanchez, C. Chappaz-Gillot, R. Salazar, H. Muguerra, E. Arbaoui, S. Berson, C. Lévy-Clément and V. Ivanova, *J. Solid State Electrochem.*, 2013, **17**, 391. d) J. Elias, R. Tena-Zaera, C. Lévy-Clément, *J. Electroanalytical Chem.*, 2008, **621** 171–177.
- 29 J. M. Kroon, N. J. Bakker, H. J. P. Smit, P. Liska, K. R. Thampi, P. Wang, S. M. Zakeeruddin, M. Grätzel, A. Hinsch, S. Hore, U. Wurfel, R. Sastrawan, J. R. Durrant, E. Palomares, H. Pettersson, T. Gruszecki, J. Walter, K. Skupien and G. Tulloch, *Prog. Photovoltaics*, 2007, **15**, 1.
- 30 Y. Wu, W. Zhu, *Chem. Soc. Rev.*, 2013, **42**, 2039; W. H. Zhu, Y. Z. Wu, S. T. Wang, W. Q. Li, X. Li, J. Chen, Z. S. Wang and H. Tian, *Adv. Funct. Mater.*, 2011, **21**, 756; M. Wang, M. Xu, D. Shi, R. Li, F. Gao, G. Zhang, Z. Yi, R. Humphry-Baker, P. Wang, S. M. Zakeeruddin and M. Grätzel, *Adv. Mater.*, 2008, **20**, 4460; H. Melhem, P. Simon, L. Beouch, F. Goubard, M. Boucharef, C. Di Bin, Y. Leconte, B. Ratier, N. Herlin-Boime and J. Bouclé, *Adv. Energy Mater.*, 2011, **1**, 908.
- 31 R. Demadrille, P. Rannou, J. Bleuse, J. – L. Oddou and A. Pron, *Macromolecules*, 2003, **36**, 7045.
- 32 Z. J. Ning, Y. Fu and H. Tian, *Energy Environ. Sci.*, 2010, **3**, 1170.
- 33 K. Keis, J. Lindgren, S. E. Lindquist and A. Hagfeldt, *Langmuir*, 2000, **16**, 4688.
- 34 H. Melhem, P. Simon, L. Beouch, F. Goubard, M. Boucharef, C. Di Bin, Y. Leconte, B. Ratier, N. Herlin-Boime and J. Bouclé, *Adv. Energy Mater.*, 2011, **1**, 908.
- 35 T. P. Chou, Q. F. Zhang and G. Z. Cao, *J. Phys. Chem. C*, 2007, **111**, 18804.
- 36 E. Guillen, J. Idigoras, T. Berger, J. Anta, C. Fernandez-Lorenzo, R. Alcantara, J. Navas and J. Martin-Calleja, *Phys. Chem. Chem. Phys.*, 2011, **13**, 207.
- 37 R. L. Willis, C. Olson, B. O'Regan, T. Lutz, J. Nelson and J. R. Durrant, *J Phys Chem B*, 2002, **106**, 7605; N. O. V. Plank, I. Howard, A. Rao, M. W. B. Wilson, C. Ducati, R. S. Mane, J. S. Bendall, R. R. M. Louca, N. C. Greenham, H. Miura, R. H. Friend, H. J. Snaith and M. E. Welland, *J. Phys. Chem. C*, 2009, **113**, 18515; M. Boucharef, C. Di Bin, M. S. Boumaza, H. J. Snaith, B. Ratier and J. Bouclé, *Nanotechnology*, 2010, **21**, 205203; N. O. V. Plank, I. Howard, A. Rao, M. W. B. Wilson, C. Ducati, R. S. Mane, J. S. Bendall, R. R. M. Louca, N. C. Greenham, H. Miura, R. H. Friend, H. J. Snaith and M. E. Welland, *J. Phys. Chem. C*, 2009, **113**, 18515.